MODELING OF COMPLEX RF/WIRELESS STRUCTURES USING COMPUTATIONALLY OPTIMIZED TIME-DOMAIN TECHNIQUES

Nathan Bushyager, Edan Dalton, and Manos Tentzeris

nbushyager@ece.gatech.edu

Georgia Institute of Technology, Atlanta, GA 30332-0250 USA

Abstract — The modeling of RF integrated structures with fine metallic details using time-domain simulators is addressed. The key features identified as difficulties in modeling metallic structures in these techniques are dielectric and metal loss and complexity of geometry. A method to model loss that involves the use of a quasi-static simulator to identify correction factors that can be applied to a time domain simulator is presented. In addition, a novel MRTD subcell method is presented that can be used to simulate fine metallic structures and other subcell effects such as the presented correction factors. An example simulation of a finely detailed structure using this technique is presented.

Keywords:- FDTD, MRTD, Time Domain Techniques, Subgridding

I. Introduction

Modern microwave structure design is becoming more difficult due to the integration of both technologies and functionalities. The decrease in size and increase in proximity of circuit elements is contributing to the inaccuracy of traditional design methodologies. In order to model devices accurately, designers are turning to full-wave simulators.

In order for full-wave simulators to be used effectively in the modeling of highly integrated microwave circuits, it is important to improve their computational efficiency

while accurately modeling the design structures. These criteria are often mutually exclusive. Several techniques [1,2] have been presented that allow the modeling of complex features that are smaller than the cell size in a given method, employing special updates and grid modifications to the cells surrounding the feature. This paper gives an overview of two new methods that have been used to model complex metallic structures as well as increase the speed of the simulation. One technique utilizes subcell modeling in the MRTD method, while the second performs corrections to the FDTD method itself. It is also shown how the FDTD based method can be performed in MRTD using the subcell MRTD method.

One of the most important elements of accurately simulating structures using time domain techniques is the modeling of metal and dielectric loss, which can determine the performance of a device and be the difference between working in simulation but failing in practice. The loss of non-dispersive dielectrics can be handled naturally in time domain methods by including a loss term in Maxwell's equations when deriving the scheme. Metal loss can be more difficult, however.

In many circuits the thickness of the metal when compared to the substrate thickness can be negligible. Due to this, it is often not practical to model metals as highly lossy substances with a finite thickness. The grid required to model these devices can easily be computationally prohibitive. In order to combat this limitation, methods exist to model the effect of a lossy metal on the circuit, while not having to simulate the metallization space to determine skin depth effects [3].

Another limitation of modeling modern structures is their physical complexity, such as multilayer modules with irregularly shaped ground planes. Time-domain

simulators utilizing cartesian grids must use small cells to represent the complex features of the devices being modeled. In recent years, the Multiresolution Time-Domain (MRTD) technique [4] has been suggested as a method to overcome many of these difficulties. The advantages of this method come from its time- and space-adaptive grid. Recently, a method that allows for the modeling of metal cells within a cell has been proposed [5].

This paper presents an overview of recent advances in the modeling of metal structures in time-domain methods that can efficiently simulate two difficult to address limitations, loss and complex geometry.

II. MRTD Background

Multiresolution time-domain is a name that has come from applying the multiresolution properties of wavelet expansion to Maxwell's time-domain curl equations. The resulting set of time domain equations is similar in many ways to the finite-difference time-domain (FDTD) technique. Due to the multiresolution nature of the MRTD, however, the method has several features that make it broader and potentially faster than FDTD.

For the purposes of this paper, a 1D derivation of the MRTD technique will be presented that explains the major features of MRTD without becoming overly complex. The equations discretized in this method are:

$$\frac{\partial}{\partial t} E_z(x,t) = \frac{1}{\varepsilon} \frac{\partial}{\partial x} H_y(x,t) \tag{1}$$

$$\frac{\partial}{\partial t} H_y(x,t) = \frac{1}{\mu} \frac{\partial}{\partial x} E_z(x,t) \tag{2}$$

To derive the method, the E and H fields are represented as a scaling and wavelet expansion of each function, and the method of moments is applied. For this paper, Haar wavelets (Figure 1) will be used. Haar wavelets have the advantage of being simple to apply; however, for this application their finite domain nature is necessary for the modeling of hard boundaries. Equations (3) and (4) are the expansions of the E and H fields in scaling functions and wavelets, (5) and (6) are the scaling function update equations for the E and H fields.

$$E_z(x) = \sum_{n,m} h_n(t)\left[{}_n E_m^{z,\phi} \varphi_m(x) + \sum_r \sum_p {}_n E_{m,r,p}^{z,\psi} \psi_{m,p}^r \right] \tag{3}$$

$$H_y(x) = \sum_{n',m'} h_{n'}(t)\left[H_{m'}^{y,\phi} \varphi_{m'}(x) + \sum_r \sum_p {}_{n'} H_{m',r,p}^{y,\psi} \psi_{m',p}^r \right] \tag{4}$$

$${}_{n'+1}H_{m'}^{y,\phi} = {}_{n'} H_{m'}^{y,\phi} + \frac{\Delta t}{\mu \Delta x}\left({}_n E_{m+1}^{z,\phi} - {}_n E_m^{z,\phi} + \sum_{r=0}^{r\max} 2^{r/2} ({}_n E_{m+1,r,0}^{z,\psi} - {}_n E_{m,r,0}^{z,\psi}) \right) \tag{5}$$

$${}_{n+1}E_m^{z,\phi} = {}_n E_m^{z,\phi} + \frac{\Delta t}{\varepsilon \Delta x}\left({}_{n'} H_{m'}^{y,\phi} - {}_{n'} H_{m'-1}^{y,\phi} + \sum_{r=0}^{r\max} 2^{r/2} ({}_{n'} H_{m'-1,r,2^r-1}^{y,\psi} - {}_{n'} H_{m',r,2^r-1}^{y,\psi}) \right) \tag{6}$$

In the above equations, $\varphi_m(x) = \varphi(x/\Delta x - m)$ and $\psi_{m,p}^r = 2^{r/2}\psi(2^r(x/\Delta x - m) - p)$, represent the scaled and translated versions of the scaling and wavelet functions. The level of wavelet resolution is r, r_{max} is the maximum resolution level to be used in the simulation. The time step is represented by n, and m represents the spatial location. The E and H fields are offset in both space and time. The location of the H fields are represented by the primed components, n'=n+1/2, m'=m+1/2^(r_{max}+2). The offset

between m and m' ensures that resolution is correctly doubled for each level of wavelet resolution added [6].

The wavelet resolution level can be varied in both space and time [7]. By applying both an absolute and relative threshold, wavelets can be tested to determine if they provide a significant contribution. This can be performed continuously during the simulation. The overall effect is to reduce the number of calculations performed compared to fixed grid techniques, because wavelet coefficients are only calculated when high field variation occurs in their vicinity.

III. MRTD Subcell Method

The novel method presented in this paper allows the simulation of a metal that overlaps only part of a cell. In standard time domain methods, such as FDTD and most MRTD methods, PEC boundaries are represented by setting the field components tangential to the metal surface to zero. One way that this can be accomplished in MRTD is to set all scaling and wavelet functions within a cell to zero. If PEC boundary conditions are applied in this manner, PEC sections must be at least the size of one cell.

If a PEC is to only overlap part of a cell, the scaling and wavelet function coefficients of the fields in a cell must add such that the fields in the area intersected by the PEC are zero. This condition must be artificially imposed on the grid after the standard electric field updates are calculated. However, this condition must be imposed such that the field magnitudes on the remainder of the cell are the same as before the condition is applied. This technique does not affect the surrounding fields, as the only fields required for the update of each electric field component are its previous value and

the values of the surrounding magnetic fields. The decoupling of the electric field components from their neighbors is implicit in the method.

Figure 2 shows a 2D Haar-MRTD cell. The cell uses a wavelet resolution of 1, which means that two levels of wavelets are used (0 and 1). The 1D scaling and wavelet functions in each direction are shown on each side. Note that the 2D scaling/wavelet functions used to represent the fields in this simulation are the products of the 1D scaling/wavelet functions. For the technique being discussed, the representation in Figure 2 is useful. However, it is important to understand that there are 2^{2R+2}=16 (for R=1) functions per field per cell.

The shaded area in the bottom half of the cell represents the PEC overlapping the cell. In order to model this cell, the E fields in the cell are first updated using the standard Haar-MRTD update equations. Next, the coefficients for the field in the cell must be altered such that the fields in the PEC region become zero without changing the field values in the non-PEC area.

A technique that allows for individual equivalent grid points to be zeroed can be derived through the use of the reconstruction matrix. The matrix, **R,** transforms the wavelet coefficients to their equivalent grid points when the scaling/wavelet coefficients and equivalent grid points [8] are treated as vectors. In Haar-MRTD there are as many coefficients as equivalent grid points, and thus **R** is square and each set of scaling/wavelet coefficients leads to a unique field distribution. The inverse of the matrix $\mathbf{R}^{-1}$, then, can be used to transform arbitrary field values into their wavelet decomposition (discrete wavelet transform). The application of a PEC then becomes a three step process. First, the **R** matrix is used to transform the wavelet values into the field values

at the equivalent grid points. Next, the field values that coincide with PEC locations are zeroed. Finally, the field values are transformed back to their wavelet coefficients using $\mathbf{R}^{-1}$ and the simulation continues. Using this method, any combination of equivalent grid points can be zeroed.

The wavelet decomposition matrix can be determined prior to simulation, therefore no matrix inversion is performed during simulation. In addition, the three step process described in the previous paragraph can be performed in one step, with one matrix multiplication. A PEC matrix, **P**, can be defined which directly transforms the wavelets from their non-PEC to PEC values. This matrix can be determined prior to simulation as,

$$\mathbf{P} = \mathbf{R}^{-1}\mathbf{R}' \tag{7}$$

In this equation **R**' is the standard reconstruction matrix, with the rows that correspond to the PEC field points set to zero.

For example, in r_{max}=0 MRTD, reconstruction can be written as

$$\begin{bmatrix} \mathbf{E}_{1,1} \\ \mathbf{E}_{1,2} \\ \mathbf{E}_{2,1} \\ \mathbf{E}_{2,2} \end{bmatrix} = \begin{bmatrix} 1 & 1 & 1 & 1 \\ 1 & 1 & -1 & -1 \\ 1 & -1 & 1 & -1 \\ 1 & -1 & -1 & 1 \end{bmatrix} \begin{bmatrix} {}_{n}\mathbf{E}_{i,j}^{x,\varphi\varphi} \\ {}_{n}\mathbf{E}_{i,j}^{x,\psi\varphi} \\ {}_{n}\mathbf{E}_{i,j}^{x,\varphi\psi} \\ {}_{n}\mathbf{E}_{i,j}^{x,\psi\psi} \end{bmatrix} \tag{8}$$

where the coordinates of the left hand **E** fields are as in Figure 3, and the right hand **E** vector represents the E scaling/wavelet coefficients.

If equivalent grid points (2,1) and (2,2) of Figure 3 are to be zeroed,

$$\mathbf{R}' = \begin{bmatrix} 1 & 1 & 1 & 1 \\ 1 & 1 & -1 & -1 \\ 0 & 0 & 0 & 0 \\ 0 & 0 & 0 & 0 \end{bmatrix} \tag{9}$$

because, as shown in (8), the third and fourth rows of the reconstruction matrix give the fields at these points. In this case

$$\mathbf{R}^{-1} = \begin{bmatrix} \frac{1}{4} & \frac{1}{4} & \frac{1}{4} & \frac{1}{4} \\ \frac{1}{4} & \frac{1}{4} & -\frac{1}{4} & -\frac{1}{4} \\ \frac{1}{4} & -\frac{1}{4} & \frac{1}{4} & -\frac{1}{4} \\ \frac{1}{4} & -\frac{1}{4} & -\frac{1}{4} & \frac{1}{4} \end{bmatrix} \tag{10}$$

and, using (7),

$$\mathbf{P} = \begin{bmatrix} \frac{1}{2} & \frac{1}{2} & 0 & 0 \\ \frac{1}{2} & \frac{1}{2} & 0 & 0 \\ 0 & 0 & \frac{1}{2} & \frac{1}{2} \\ 0 & 0 & \frac{1}{2} & \frac{1}{2} \end{bmatrix} \tag{11}$$

It is clear that if no PEC is applied, **R'=R** and **P** is the identity matrix. Using the PEC matrix, **P**

$$\mathbf{}_{n}\mathbf{E}^{x}_{i,j,PEC} = \mathbf{P}\,\mathbf{}_{n}\mathbf{E}^{x}_{i,j} \tag{12}$$

If this matrix is used in the case of the previous example, the coefficients contained in $\mathbf{}_{n}\mathbf{E}^{x}_{i,j,PEC}$ will be different than those in $\mathbf{}_{n}\mathbf{E}^{x}_{i,j}$; however they will reconstruct to the same values at all points in Figure 3 except for (2,1) and (2,2), where they will reconstruct to 0. If the **P** matrices are determined prior to simulation, the application of PEC at arbitrary equivalent grid points becomes a matter of matrix multiplication in each cell that contains a PEC.

This technique has other direct applications to MRTD. The application of any condition that requires the modification of the field values at individual grid points can be performed using this approach. For example, an arbitrary value can be added to any equivalent grid point in order to simulate source conditions. Using this decomposition technique, the excitation can be finely shaped to match a desired mode.

IV. Hybrid Method

An alternative technique that improves the accuracy of the simulator in the areas of metals involves the hybridization of FDTD and an electrostatic/magneto-quasistatic solver. The hybrid modeling technique presented here uses the quasistatic field solvers to determine the potential/surface currents over lossy/metal surfaces (e.g. a ground plane in a packaged microsystem) [9,10]. The solution from the quasistatic field solver is then used to calculate correction factors for an FDTD grid, which are applied to the time-domain solver to increase the accuracy of the finite-difference equations. The fine grid used by the static field solver also displays clearly the areas of the fastest field variation, so that the FDTD solver can take advantage of the evidential knowledge of the steady-state fields by incorporating adaptive gridding, while areas of low field variation can be simulated with a much coarser grid.

The combination of the static solver and the FDTD method is an attempt to resolve some of the difficulties associated with modeling highly conductive, thin materials in the time domain. Researchers often rely on “common sense” approaches to generate the mesh for full-wave simulation, and this can result in inaccuracy in areas of high field variation. The static solver is used in conjunction with a variable-grid FDTD mesh to reduce errors due to mesh size near structure discontinuities. One of the main advantages of the static solver is that, since it has no time-marching component, it does not take as long to process as a dynamic simulation of comparable resolution. In addition, it can be used as a preprocessing step that can optimize the mesh for the full-wave simulation.

In order to integrate the quasistatic solver with the FDTD algorithm, correction factors are calculated based on the static field distributions. This is accomplished by the use of the quasistatic solvers to calculate the field distribution over the static mesh. These field values are used as the components of the integral approximation of Faraday's and Ampere's laws (13), (14).

$$\oint_l \vec{E} \cdot d\vec{l} = -\frac{d}{dt} \iint_A \mu \vec{H} \cdot d\vec{A} \tag{13}$$

$$\oint_l \vec{H} \cdot d\vec{l} = \frac{d}{dt} \iint_A \varepsilon \vec{E} \cdot d\vec{A} \tag{14}$$

Once the quasistatic fields have been calculated, the field component at the center of the dynamic grid cell (as shown in Figure 4) is used to calculate the dynamic grid integral approximation for use in the calculation of the correction factors. The expressions for the two types of correction factors, using generic field components, are given in (16) and (17), where CF_l represents the line integral correction factor, CF_A represents the surface integral correction factor, and the Δ-terms represent the sizes of the coarse FDTD cells around which the integrals are discretized using the quasistatic values. The F values in the numerators of the correction factor expressions are the quasistatic field values over the number of static cells that occupy the discretized integration area. In the denominator, the F values are the quasistatic value at the exact location it occupies at the coarse-mesh FDTD cell, shown by the dots in the middle of the dynamic cells in Figure 4.

$$CF_l = \frac{\int \vec{F} \cdot d\vec{l}}{\overline{F} \cdot \Delta l} \tag{16}$$

$$CF_A = \frac{\iint \vec{F} \cdot d\vec{x} \cdot d\vec{y}}{\overline{F} \cdot \Delta x \cdot \Delta y} \tag{17}$$

The magnitude of the correction factors comes from the difference between the field integral approximations over the two different grids. As can be surmised from Figure 4, in areas of very high field variation, the different resolutions can produce large magnitudes of correction factors.

Following the derivation of the FDTD update equations from the integral forms of Maxwell's equations [11] and incorporating the correction factor terms in the formulation, the update expressions for H_x and E_x are derived as shown in (18) and (19) (conductivity terms and nonessential subscripts are omitted for simplicity).

$$E_x\big|_{j,k}^{n+1} = E_x\big|_{j,k}^{n} + \frac{2\Delta t}{\varepsilon \cdot CFA_{Ex}\big|_{j,k}} \left(\frac{CFL_{Hz}\big|_{j+.5,k} \cdot H_z\,|_{j+.5,k}^{n+.5} - CFL_{Hz}\big|_{j-.5,k} \cdot H_z\,|_{j-.5,k}^{n+.5}}{\Delta y} - \frac{CFL_{Hy}\big|_{j,k+.5} \cdot H_y\,|_{j,k+.5}^{n+.5} - CFL_{Hy}\big|_{j,k-.5} \cdot H_y\,|_{j,k-.5}^{n+.5}}{\Delta z} \right) \tag{18}$$

$$H_x\big|_{j-.5,k-.5}^{n+.5} = H_x\big|_{j-.5,k-.5}^{n-.5} + \frac{2\Delta t}{\mu \cdot CFA_{Hx}\big|_{j-.5,k-.5}} \left(\frac{CFL_{Ey}\big|_{j,k} \cdot E_y\,|_{j,k}^{n} - CFL_{Ey}\big|_{j,k-1} \cdot E_y\,|_{j,k-1}^{n}}{\Delta z} - \frac{CFL_{Ez}\big|_{j,k} \cdot E_z\,|_{j,k}^{n} - CFL_{Ez}\big|_{j-1,k} \cdot E_z\,|_{j-1,k}^{n}}{\Delta y} \right) \tag{19}$$

The relationship of the field components and the approximations of the integral equations can be seen in Figure 5, which shows the contours and surfaces used in this calculation. The contour integral of the electric field is related to the surface integral of the magnetic field by Faraday's law. In this illustration, the surface integration of the H_x field is related to the integral of the contour including the E_x and E_y field components. The relation for the E_x field is similar, and the derivation is the same.

The end result of this hybridization is that a given structure can be simulated in less time than with conventional FDTD. The coupling with the quasistatic solver reduces the computational load by allowing the use of a coarser FDTD grid while regaining some of

the accuracy lost by correcting discretization errors in the dynamic simulation. In addition, there is very little alteration to the standard FDTD algorithm. The only addition is the insertion of the correction factors in the field update equations, which are determined prior to the FDTD simulation, and will not add extra execution time to the dynamic simulation. And, as previously stated, since the quasistatic solver involves no time-stepping, it takes much less time to run than the dynamic solver. One of the few disadvantages of the hybrid method is a necessary reduction in the time step size due to the introduction of the correction factors in the update equations. Since the fields are multiplied by numbers that can be larger than one, the stability of the scheme can be compromised if the time step used is close to the Courant limit. This phenomenon can be countered by reducing the time step in proportion to the magnitude of the largest correction factors.

V. Hybrid Method in MRTD

The hybrid method presented above can also be applied directly to MRTD. Using the subcell modeling method that was shown for PECs, the hybrid method can be easily applied in MRTD. This method can be demonstrated by examining the 2D MRTD update equations. For the 2D TE_z mode, the update equation for the E_x field is [5],

$$\mathbf{E}^{x}_{i,j\,n} = \mathbf{E}^{x}_{i,j\,n-1} + \frac{\Delta t}{\varepsilon \Delta y}\left(\mathbf{U}_{E_{x1}\,n-1}\mathbf{H}^{z}_{i,j} + \mathbf{U}_{E_{x2}\,n-1}\mathbf{H}^{z}_{i,j-1}\right) \tag{20}$$

In the above equation, **E** and **H** are the vector of scaling/wavelet coefficients as in (8). The **U** matricies represent the inner products of scaling/wavelet coefficients.

In (20) the E scaling/wavelet coefficients are directly determined from the H scaling/wavelet coefficients. However, the correction factors determined from the hybrid

method must be directly multiplied with field values. In order to apply these correction factors, the equation must be converted to a pointwise form. This can be accomplished by multiplying (20) with the reconstruction matrix,

$$\mathbf{R}_n \mathbf{E}^x_{i,j} = \mathbf{R}_{n-1} \mathbf{E}^x_{i,j} + \frac{\Delta t}{\varepsilon \Delta y} \left(\mathbf{U}'_{E_{x1}\, n-1} \mathbf{R}_{n-1} \mathbf{H}^z_{i,j} + \mathbf{U}'_{E_{x2}\, n-1} \mathbf{R}_{n-1} \mathbf{H}^z_{i,j-1} \right) \tag{21}$$

noting

$$\mathbf{H}^z_{i,j} = \mathbf{R}^{-1} \mathbf{R} \mathbf{H}^z_{i,j} \tag{22}$$

and defining

$$\mathbf{U}' = \mathbf{R} \mathbf{U} \mathbf{R}^{-1} \tag{23}$$

In this form, $\mathbf{R}_n \mathbf{E}^x_{i,j}$ is the vector of pointwise E fields and $\mathbf{R}_{n-1} \mathbf{H}^z_{i,j}$ is the vector of pointwise H fields. To apply the correction factors, a matrix **C** of correction factors must be multiplied by each **H** field vector in (21)

$$\mathbf{R}_n \mathbf{E}^x_{i,j} = \mathbf{R}_{n-1} \mathbf{E}^x_{i,j} + \frac{\Delta t}{\varepsilon \Delta y} \left(\mathbf{C}_1 \mathbf{U}'_{E_{x1}\, n-1} \mathbf{R}_{n-1} \mathbf{H}^z_{i,j} + \mathbf{C}_2 \mathbf{U}'_{E_{x2}\, n-1} \mathbf{R}_{n-1} \mathbf{H}^z_{i,j-1} \right) \tag{24}$$

The **C** matrix has the correction factors on the diagonal, and zeroes in the off diagonal elements. When multiplied, then, each of the H fields is individually modified by the corresponding element of the **C** matrix. Next (24) can be multiplied by $\mathbf{R}^{-1}$ to convert back to scaling/wavelet form. The resulting equation,

$$_n \mathbf{E}^x_{i,j} = _{n-1} \mathbf{E}^x_{i,j} + \frac{\Delta t}{\varepsilon \Delta y} \left(\mathbf{U}^C_{E_{x1}\, n-1} \mathbf{H}^z_{i,j} + \mathbf{U}^C_{E_{x2}\, n-1} \mathbf{H}^z_{i,j-1} \right) \tag{25}$$

gives a direct update of the scaling/wavelet coefficients if

$$\mathbf{U}^C = \mathbf{R}^{-1} \mathbf{C} \mathbf{U}' \mathbf{R} \tag{26}$$

To apply this method to MRTD, $\mathbf{U}^C$ must be determined in a preprocessing step. Once determined, the update equations are exactly the same as standard MRTD. The

method adds no overhead to the MRTD update scheme. This is an excellent example of how the MRTD PEC subcell scheme previously presented can be used to apply other subcell effects.

VI. Example – PEC Screen

One important application of this method is the simulation of arbitrarily shaped PEC structures, such as EBG and via-array based geometries (e.g cavities and crosstalk-reducing via-array walls). For this purpose, a parallel plate waveguide intersected by a PEC screen was simulated.

The structure being modeled in this example is presented in Figure 6. This structure is a parallel plate waveguide that is intersected by metal planes with small apertures. This structure is analogous to structures used in many modern multilayer substrate technologies, in either via fences or patterned ground planes. While not offering a significant practical benefit, it allows both a demonstration of the simulation method and an effective comparison to FDTD.

The structure was first simulated in a 2D, $r_{max}=2$, MRTD scheme. Figure 7 shows a detailed view of the grid of the first four walls of the PEC screen. The shaded cells show where the PEC boundary condition is applied. This structure was then simulated in FDTD using an identical grid. The time domain output voltage from both simulations is presented in Fig. 8, an excellent agreement can be seen. The difference between the output voltage of the two simulations, normalized to the maximum voltage, is presented in Figure 9. The size of this error indicates that the schemes are identical and differences are due to numerical round off error.

In order to demonstrate how this technique can be used to achieve true adaptive gridding, another simulation was performed. In this simulation, the maximum wavelet resolution $r_{max}=2$ is only used in screen area of the grid and the surrounding two cells. Outside of this area, $r_{max}=1$ is used, which represents the largest equivalent cell spacing that yields acceptable numerical dispersion for this case. The time domain output of this case is presented in Figure 8. Unlike the FDTD/MRTD comparison, these schemes are not equivalent and very small, but observable, differences occur. The magnitude of the difference between the schemes, normalized to peak output voltage, is presented in Figure 10. The $r_{max}=1$ grid has lower resolution, however results are very close to those of the $r_{max}=2$ grid. The $r_{max}=1$ case, however uses 48 fewer grid points per field per cell, and thus represents both a memory and execution efficiency of 75% over the $r_{max}=2$ and FDTD case.

VII. Conclusion

The modeling of conductors in time domain often leads to many difficulties. Either by trying to match a grid to a complex shape or accurately modeling loss, it is often a requirement to sacrifice time for accurate results. Two methods were presented in this paper that allow for the modeling of these structures while offering improved speed when compared to similar methods. The subcell MRTD method provides a framework that can be used to model features that are smaller than an MRTD cell. This is demonstrated with both PECs and the hybrid correction factors. Using this technique, the full advantages of the MRTD time- and space-adaptive grid can be realized for finely detailed structures. In addition, the loss and inaccuracies associated with metal simulation can be treated in a

simple way. Finally, these techniques can be easily added to existing codes, allowing improvements in efficiency that do not require large amounts of code rewriting.

VIII. Acknowledgements

The authors wish to acknowledge the support of the Georgia Tech NSF Packaging Research Center, The Yamacraw Design Center of the State of Georgia, and NSF CAREER Grant# 9984761.

Figures

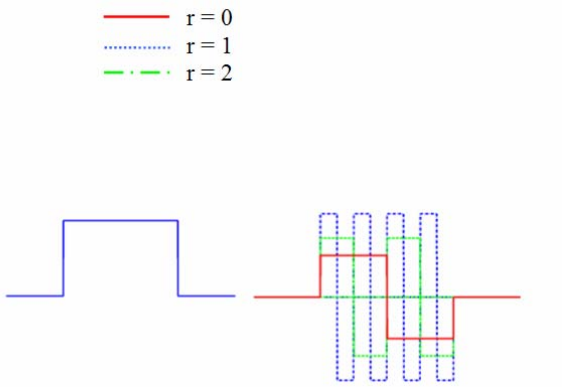

Figure 1:Haar scaling function (φ, left), 0^{th}, 1^{st}, and 2^{nd} resolution wavelets (ψ, right)

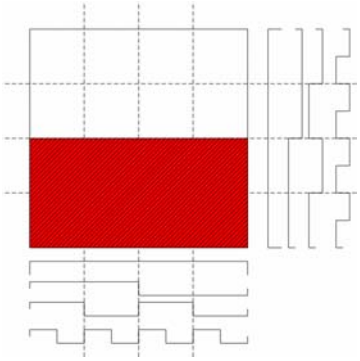

Figure 2: 2D Haar-MRTD-1 cell showing half metallization

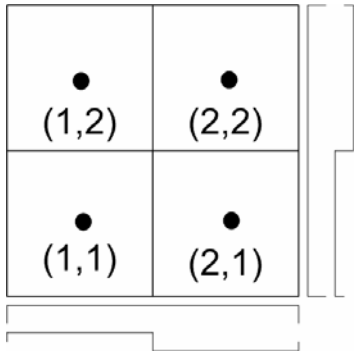

Figure 3: Equivalent grid points of 2D MRTD cell with $r_{max}=0$

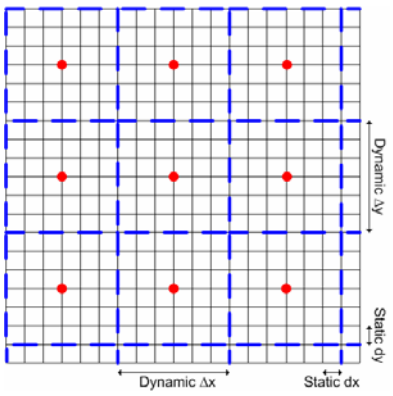

Figure 4: Orientation and alignment of the static and dynamic grids

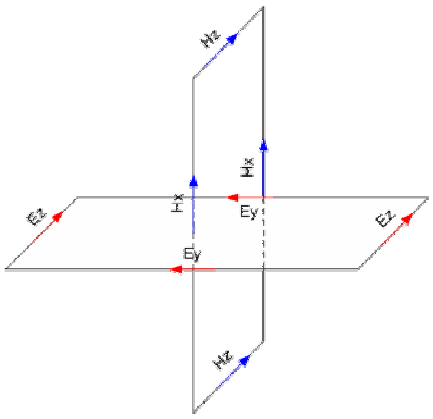

Figure 5: Faraday contour showing the field relations for the calculation of the Hx field

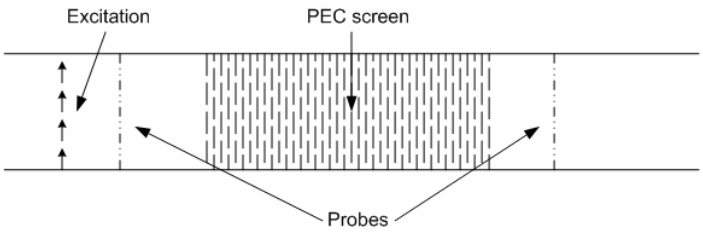

Figure 6: Parallel plate waveguide with PEC screen

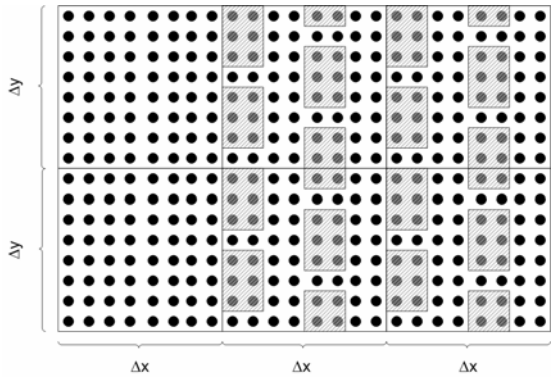

Figure 7: Cells in screen area for parallel plate waveguide with PEC screen

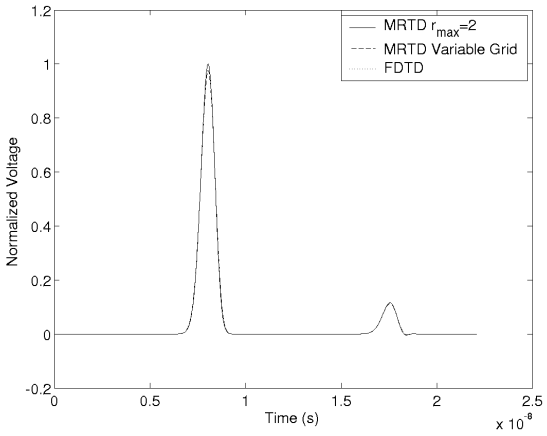

Figure 8: Time domain output voltage for parallel plate waveguide with PEC screen, FDTD/MRTD/MRTD variable grid comparison

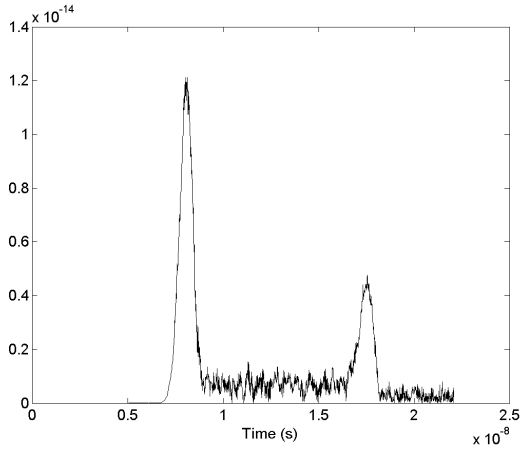

Figure 9: Magnitude of difference between MRTD and FDTD parallel plate waveguide with PEC screen output voltage (normalized to maximum voltage)

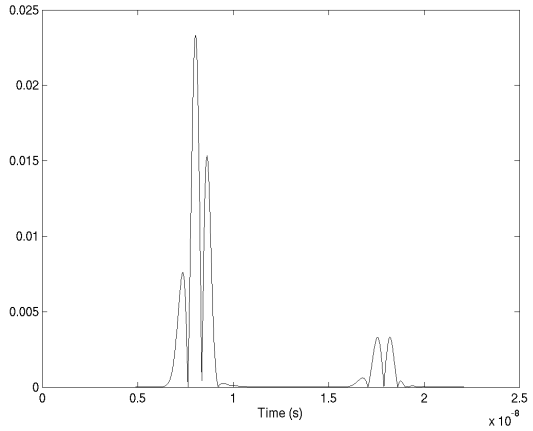

Figure 10: Magnitude of difference between MRTD and MRTD variable grid parallel plate waveguide with PEC screen output voltage (normalized to maximum voltage)

References

[1] M. Celuch-Marcysiak, “Local stereoscopic field singularity models for FDTD analysis of guided wave problems”, *Proc. of the 2003 IEEE IMS*, pp. 1137-1140, Philadelphia, PA, June 2003.

[2] U. Mueller, P.P.M. So, W.J.R. Hoefer, “The compensation of coarseness error in 2D TLM modeling of microwave structures,” *Proc. of the 1992 IEEE IMS*, pp. 373-376, Albuquerque, NM, June 1992.

[3] J.H. Beggs, R.J. Luebbers, K.S. Yee, K.S. Kunz, “Finite-difference time-domain implementation of surface impedance boundary conditions”, *IEEE Trans Antennas Prop.*, Vol. 40, pp. 49-56, Jan. 1992.

[4] M. Krumpholz, L. P. B. Katehi, "MRTD: New time domain schemes based on multiresolution analysis", IEEE Trans. Microwave Theory Tech., vol.44, pp.555-561 , Apr. 1996.

[5] N. Bushyager, M. Tentzeris, “Composite cell MRTD method for the efficient simulation of complex microwave structures”, *Proc. 2003 EUMC,* Munich, Germany, October 2003.

[6] T. Dogaru, L. Carin, “Application of Haar-wavelet-based multiresolution time-domain schemes to electromagnetic scattering problems,” *IEEE Trans. Antennas Prop.*, Vol. 50, No 2, pp. 774-784, June, 2002.

[7] E.Tentzeris, A.Cangellaris, L.P.B.Katehi, J.Harvey, "Multiresolution time-domain (MRTD) adaptive schemes using arbitrary resolutions of wavelets", *IEEE Trans. MTT*, Vol.50, No.2, pp.501-516, March 2002.

[8] C. Sarris and L. P. B. Katehi, “Fundamental gridding-related dispersion effects in multiresolution time-domain schemes,” IEEE Trans. Microwave Theory Tech, vol. 49, no. 12, pp 2248-2257, Dec. 2001.

[9] D. B. Shorthouse and C.J. Railton, "The incorporation of static field solutions into the finite difference time domain algorithm," IEEE Trans on Microwave Theory and Techniques, Vol. 40, pp. 986-994, May 1992.

[10] M. Kunze and W. Heinrich, "3D hybrid finite-difference method for lossy structures based on quasi-static field solutions," *Proc. of the 2002 IEEE IMS*, pp. 1881-1884, Seattle, WA, June 2002.

[11] A. Taflove and S. Hagness Computational Electrodynamics: The Finite Difference Time Domain Method, Norwood, MA: Artech House, 1995.